ISSN 1070-3284, Russian Journal of Coordination Chemistry, 2021, Vol. 47, No. 9, pp. 610–619. © Pleiades Publishing, Ltd., 2021.
Russian Text © The Author(s), 2021, published in Koordinatsionnaya Khimiya, 2021, Vol. 47, No. 9, pp. 552–561.

Metal–Organic Frameworks of Magnesium Based on 2,5-Dihydroxy-3,6-di-*tert*-butyl-*para*-benzoquinone

O. Yu. Trofimova[a], I. V. Ershova[a], A. V. Maleeva[a], I. A. Yakushev[b, c], P. V. Dorovatovskii[c], R. R. Aisin[d], and A. V. Piskunov[a, *]

[a] *Razuvaev Institute of Organometallic Chemistry, Russian Academy of Sciences, Nizhny Novgorod, Russia*
[b] *Kurnakov Institute of General and Inorganic Chemistry, Russian Academy of Sciences, Moscow, 119991 Russia*
[c] *Kurchatov Institute Russian Research Center, Moscow, 123182 Russia*
[d] *Nesmeyanov Institute of Organoelement Compounds, Russian Academy of Sciences,Moscow, 119991 Russia*
**e-mail: pial@iomc.ras.ru*

Received January 27, 2021; revised February 25, 2021; accepted March 1, 2021

Abstract—New one-dimensional metal–organic frameworks of magnesium $[Mg(pQ)\cdot 2DMF]_n$ (**I**), $[Mg(pQ)\cdot 2DMAA]_n$ (**II**), and $[Mg(pQ)\cdot 2(NMP)]_n$ (**III**) (pQ is the 2,5-dihydroxy-3,6-di-*tert*-butyl-*para*-benzoquinone dianion) are synthesized by the solvothermal method in different solvents (*N*,*N*-dimethylformamide (DMF), *N*,*N*-dimethylacetamide (DMAA), and *N*-methyl-2-pyrrolidone (NMP)). The crystal structures of compounds **I** and **III** are determined by X-ray structure analysis (CIF files CCDC nos. 2058147 (**I**) and 2058148 (**II**)). The spectral characteristics and thermal stability of the synthesized metal–organic frameworks are studied.

Keywords: anilate ligand, metal–organic frameworks, redox-active ligand, thermogravimetric analysis, X-ray structure analysis, solvothermal synthesis

DOI: 10.1134/S1070328421090086

INTRODUCTION

Metal–organic frameworks (MOF) represent a new class of microporous materials built on metal cations or clusters linked by bridging ligands into one-dimensional chains, two-dimensional layers, or three-dimensional carcasses. The MOF are characterized by a range of unique properties that provide their potential application in various spheres. Materials based on MOF can be used as gas adsorbents [1, 2]; luminescent [3, 4], electrochemical, or photophysical sensors [5, 6]; and optical [7], electroconducting [8, 9], and magnetic materials [10–14]. One of the promising trends for the synthesis of the MOF with the unique properties is the production of redox-active metal-organic frameworks [8, 9, 15]. The physical and chemical properties, crystal structures, and topology of the MOF depend on the nature of metal ions and organic ligands involved in their building. The anilate ligands (2,5-dihydroxy-1,4-benzoquinone derivatives) containing various substituents in positions 3 and 6 (H, Cl, Br, I, CN, NO_2, etc.) are used most frequently as redox-active bridging ligands [8, 16–18]. Being bound in a complex with the metal of this type compound, they can exist in four different oxidation–reduction states (Scheme 1). The dianion can be characterized by the *o*-quinoid distribution of bond lengths and, correspondingly, the type of binding with the complexing agent in which negative charges are concentrated on the adjacent oxygen atoms.

Among the group of anilate ligands, the coordination properties of 2,5-dihydroxy-3,6-di-*tert*-butyl-*para*-quinone (H_2pQ) [19] are studied rather poorly. Only several articles reported on the synthesis of the mononuclear triphenylantimony(V) derivatives $pQSbPh_3\cdot CH_3OH$, and $Et_3NH[pQSbPh_3Br]$ [20] and on the binuclear tin, nickel, iron, and cobalt based on this ligand [19, 21, 22] have been published to the recent time. Nevertheless, the redox-active nature of this dihydroxy-*para*-quinone made it possible to demonstrate the perspective properties of the metal complexes involving this quinone. For example, the binuclear iron compounds are characterized by the spin–spin transition in a range of ambient temperatures [22], and the cobalt derivative exhibits the phenomenon of induced electron transfer [21]. No attempts to synthesize MOF with this anilate ligand have been made up to recently. The first MOF containing the H_2pQ dianion as bridging ligands covalently binding lanthanide ions into 2D cross-linked structures were synthesized and characterized only in 2020 [23]. New linear magnesium MOF based on H_2pQ, namely, $[Mg(pQ)\cdot 2DMF]_n$ (**I**), $[Mg(pQ)\cdot 2DMAA]_n$ (**II**), and $[Mg(pQ)\cdot 2(NMP)]_n$ (**III**), were synthesized in this work.

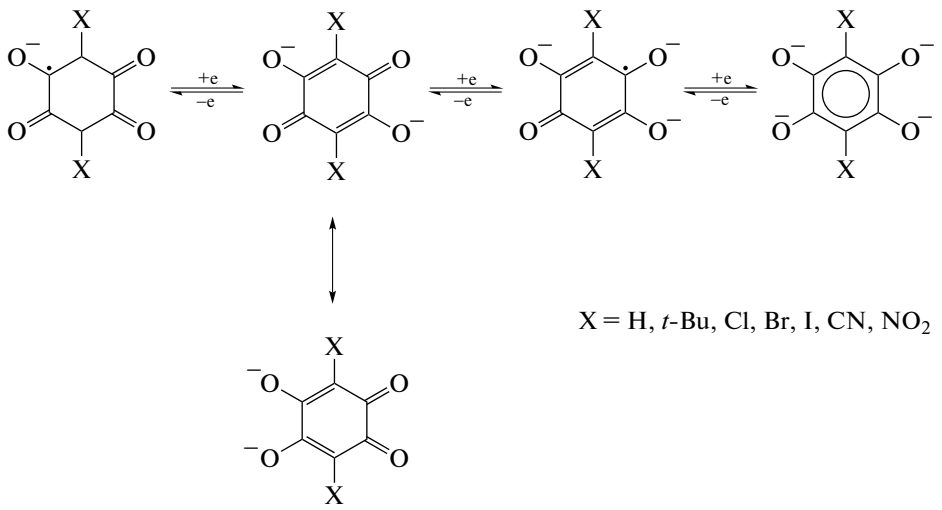

Scheme 1.

EXPERIMENTAL

IR spectra were recorded on an FSM-1201 FT-IR spectrometer (suspensions in Nujol, KBr cells). Electronic absorption spectra (EAS) were recorded on a Carl Zeiss Jena Specord M400 spectrometer (in Nujol). Elemental analysis was carried out on an Elementar Vario El cube instrument. The studies by differential scanning calorimetry (DSC) and thermogravimetric analysis (TG) of the compounds were carried out on a Mettler Toledo TGA/DSC3+ instrument at 30–500°C in a nitrogen atmosphere (crucible of polycrystalline alumina) with a heating rate of 5°C/min. The following commercial reagents were used: *N*,*N*'-dimethylformamide (DMF), *N*,*N*-dimethylacetamide (DMAA), *N*-methyl-2-pyrrolidone (NMP), and $MgCl_2 \cdot 6H_2O$. Ligand H_2pQ was synthesized using a known procedure [19].

Synthesis of complexes I–III. A mixture of $MgCl_2 \cdot 6H_2O$ (0.04 mmol) and H_2pQ (0.04 mmol) was dissolved in 5 mL of the corresponding solvent (DMF for **I**, DMAA for **II**, and NMP for **III**), and the solution was heated in a sealed ampule at 130°C for 24 h. The formed bright colored crystals of complexes **I–III** were collected on a Schott filter, washed with the pure solvent, and dried in air.

MOF **I**: pink large needle-like crystals. The yield was 82%.

For $C_{20}H_{32}N_2O_6Mg$

Anal. calcd., %	C, 57.09	H, 7.67	N, 6.66
Found, %	C, 56.96	H, 7.63	N, 6.15

IR (ν, cm^{-1}): 1688 s, 1668 s, 1608 w, 1541 s, 1480 s, 1442 s, 1420 m, 1361 w, 1259 m, 1198 m, 1110 s, 1065 w, 1049 w, 970 m, 927 m, 902 s, 868 m, 801 w, 790 m, 685 s, 627 m, 525 s. EAS (λ, nm): 320, 340, 515.

MOF **II**: pink fine needle-like crystals. The yield was 75%.

For $C_{22}H_{36}N_2O_6Mg$

Anal. calcd., %	C, 58.87	H, 8.08	N, 6.24
Found, %	C, 58.70	H, 8.13	N, 5.86

IR (ν, cm^{-1}): 1657 s, 1627 s, 1538 s, 1344 s, 1269 s, 1218 m, 1192 s, 1048 m, 1038 m, 1026 s, 970 m, 925 w, 904 s, 851 w, 803 w, 791 w, 748 m, 657 s, 627 m, 610 s, 596 m, 523 s, 505 m, 478 w. EAS (λ, nm): 320, 345, 510.

MOF **III**: vinous fine needle-like crystals. The yield was 78%. According to the elemental analysis data, compound **II** contains 0.5 molecule of occluded *N*-methyl-2-pyrrolidone based on one $[Mg(pQ) \cdot 2(NMP)]_n$ unit.

For $C_{26.5}H_{40.5}N_{2.5}O_{6.5}Mg$

Anal. calcd., %	C, 60.93	H, 7.81	N, 6.70
Found, %	C, 60.88	H, 7.83	N, 6.58

IR (ν, cm^{-1}): 1699 s, 1664 s, 1540 s, 1344 s, 1309 m, 1262 m, 1222 w, 1199 m, 1176 m, 1117 s, 1207 w, 1052 m, 989 m, 972 m, 928 m, 902 s, 853 w, 792 m, 755 m, 657 s, 629 w, 564 w, 526 s, 472 m. EAS (λ, nm): 310, 335, 490.

Quantum-chemical calculations were performed using the Gaussian09 program package [24] by the density functional theory (DFT) with the B3LYP functional [25] and the standard 6-311+(d,p) basis set for all atoms.

X-ray structure analysis (XSA). The X-ray diffraction data for MOF **I** and **III** were obtained on the Belok beamline at the Kurchatov specialized source of synchrotron radiation of the Kurchatov Institute Russian Research Center (Moscow, Russia) in the φ scan mode using a Rayonix SX165 CCD detector at 100 K (λ = 0.79313 and 0.79312 Å for **I** and **III**, respectively) [26]. The primary indexing was performed, the unit cell parameters were refined, the reflections were integrated, and an absorption correction of reflection intensities was applied using the XDS software [27]. The structures were solved by direct methods and refined in the anisotropic approximation by full matrix least squares for F^2 for all non-hydrogen atoms. Since the *tert*-butyl group is disordered over two positions (ratio of populations of atomic positions 0.882 : 0.118), as well as coordinated *N*-methyl-2-pyrrolidone in the structure of complex **III** (ratio of populations of atomic positions 0.749 : 0.251), the SADI geometric restraints were used in both cases in the refinement of the model of minor components of the disordered groups, and the FLAT restraints and the SIMU and RIGU restraints for thermal shifts of atoms were used for *N*-methyl-2-pyrrolidone only. In the case of complex **I**, the hydrogen atoms were revealed from the electron density map and refined in the isotropic approximation. In the case of complex **III**, the hydrogen atoms were placed in the calculated positions and refined by the riding model with $U_{iso}(H) = 1.5U_{equiv}(C)$ for the hydrogen atoms of the methyl groups and $1.2U_{equiv}(C)$ for other hydrogen atoms. The calculations were performed using the SHELXTL software [28] in the OLEX2 medium of structural data visualization and processing [29].

The crystallographic data for compounds **I** and **III** were deposited with the Cambridge Crystallographic Data Centre (CIF files CCDC nos. 2058147 and 2058148, respectively; deposit@ccdc.cam.ac.uk or http://www.ccdc.cam.ac.uk/data_request/cif).

RESULTS AND DISCUSSION

Three linear magnesium MOF based on H_2pQ were synthesized by the solvothermal method in different solvents (DMF, DMAA, and NMP). The reaction occurs in a sealed glass ampule on heating to 130°C for 24 h. As a result, the $[Mg(pQ)\cdot 2DMF]_n$ (**I**), $[Mg(pQ)\cdot 2DMAA]_n$ (**II**), and $[Mg(pQ)\cdot 2(NMP)]_n$ (**III**) derivatives (pQ is the 2,5-dihydroxy-3,6-di-*tert*-butyl-*para*-benzoquinone dianion) (Scheme 2) were obtained. Vinous pink crystalline compounds **I**–**III** are formed during the synthesis and further cooling in the reaction mixture in the yields close to quantitative. After washing on a filter with the same solvent that was used in the synthesis and further drying in air, the synthesized MOF were analytically pure. According to the elemental and TG analyses data (see below), complex **III** contains 0.5 pyrrolidone molecule per unit of the polymeric chain. The synthesized compounds are insoluble in water and organic solvents and resistant to air oxygen and moisture.

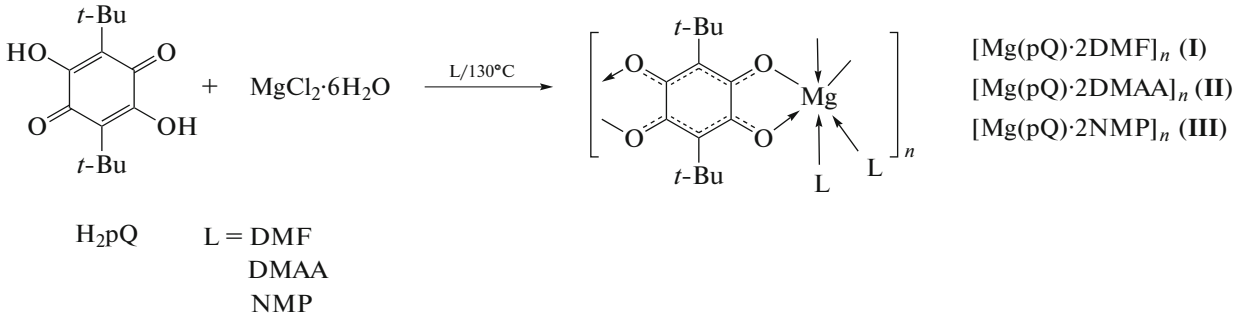

Scheme 2.

The structures of MOF **I** and **III** were determined by XSA. The compositions and chemical purity of all compounds were confirmed by IR spectroscopy and TG and elemental analyses. The molecular structures of compounds **I** and **III** are presented in Figs. 1 and 2. The crystallographic data and X-ray diffraction experimental parameters are given in Table 1. Selected bond lengths are listed in Table 2.

According to the XSA data, MOF **I** and **III** represent one-dimensional polymers (Fig. 1). Compound **I** crystallizes in the monoclinic symmetry group *C*2/*c*, and derivative **III** crystallizes in the monoclinic symmetry group $P2_1/c$. The topology of the chain of both derivatives is 2C1. The coordination environment of each magnesium cation in compounds **I** and **III** is a distorted octahedron containing four oxygen atoms of two chelating pQ^{-2} ligands and two oxygen atoms of the coordinated solvent molecules at the vertices (Figs. 2, 3). The *cis* arrangement of the ligands in the coordination sphere of the metal leads to the sigzag structure of the polymeric chains. An analysis of the crystal structures of complexes **I** and **III** by the construction of the Hirshfeld surface using the Crystal

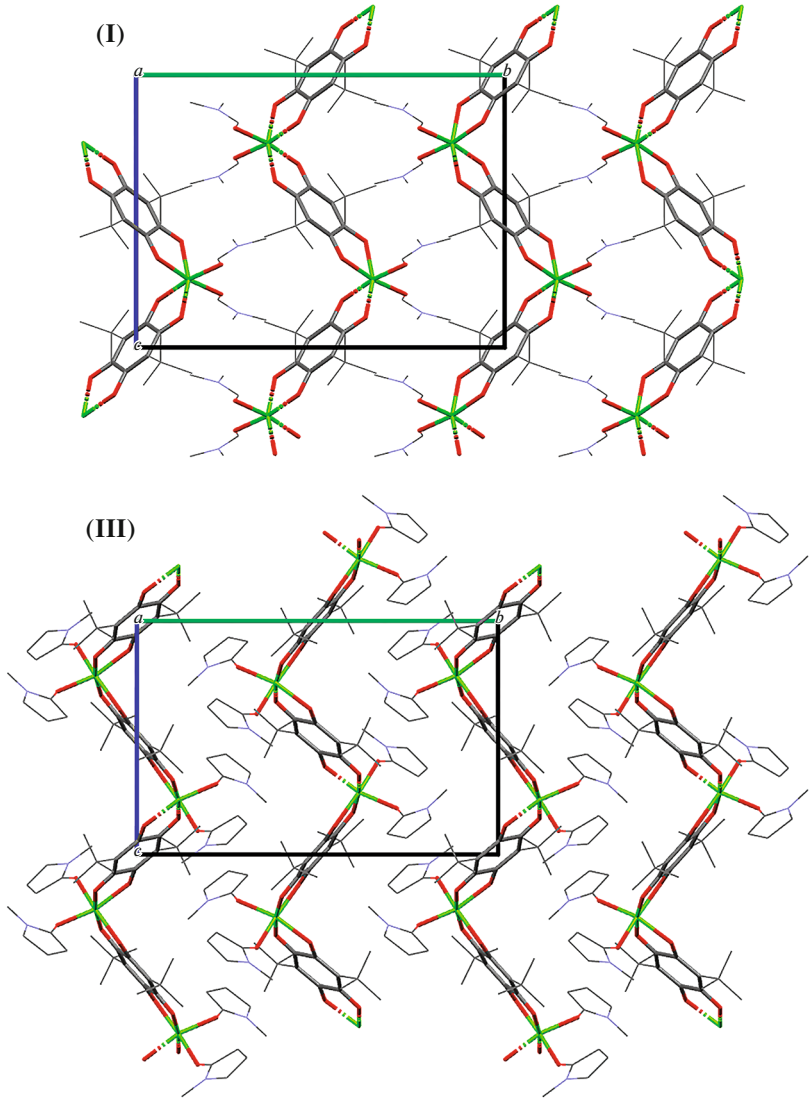

Fig. 1. Views of the linear structures of MOF **I** and **III** along the *a* axis.

Explorer 17.5 program package [30] revealed no significant intermolecular interactions between the chains.

In both MOF, the pQ^{2-} dianion has a similar structure and demonstrates two delocalized π-electron anionic systems linked to each other by the ordinary C(1)–C(3) and C(8)–C(10) bonds (for compound **III**) through the middles of which the symmetry element passes. In compound **I**, the C(1)–C(2) and C(2)–C(3) bonds, as well as C(1)–O(1) and C(3)–O(2), are nearly equal, indicating a very high charge delocalization over these moieties of the ligand. The C(1)–C(2) and C(2)–C(3) bond lengths lie in the range characteristic of classical aromatic carbon–carbon bonds. The C(1)–O(1) and C(3)–O(2) interatomic distances are intermediate between the values for double and ordinary oxygen–carbon bonds, whereas they are much shorter than those observed in the related magnesium *o*-semiquinone derivatives [31, 32]. Derivative **III** is characterized by a similar charge delocalization in the organic ligand, but the bond length averaging and, hence, delocalization are somewhat lower. For example, the O(1)–C(1) and O(6)–C(10) bonds are slightly longer than the corresponding O(2)–C(3) and O(5)–C(8) bonds, whereas the C(1)–C(2) and C(8)–C(9) bonds in the quinoid ring are slightly shorter than C(3)–C(2) and C(10)–C(9). This electron density delocalization is characteristic of the anilate ligands performing the bridging function in the metal complexes. The above described bond length distribution in the pQ^{2-} dianionic fragment differs cardinally from that observed for the mononuclear triphenylantimony(V) complex [20] for which the distinctly pronounced *o*-quinoid type of alternation of the C–C and C–O bond lengths in the redox-active ligand was observed.

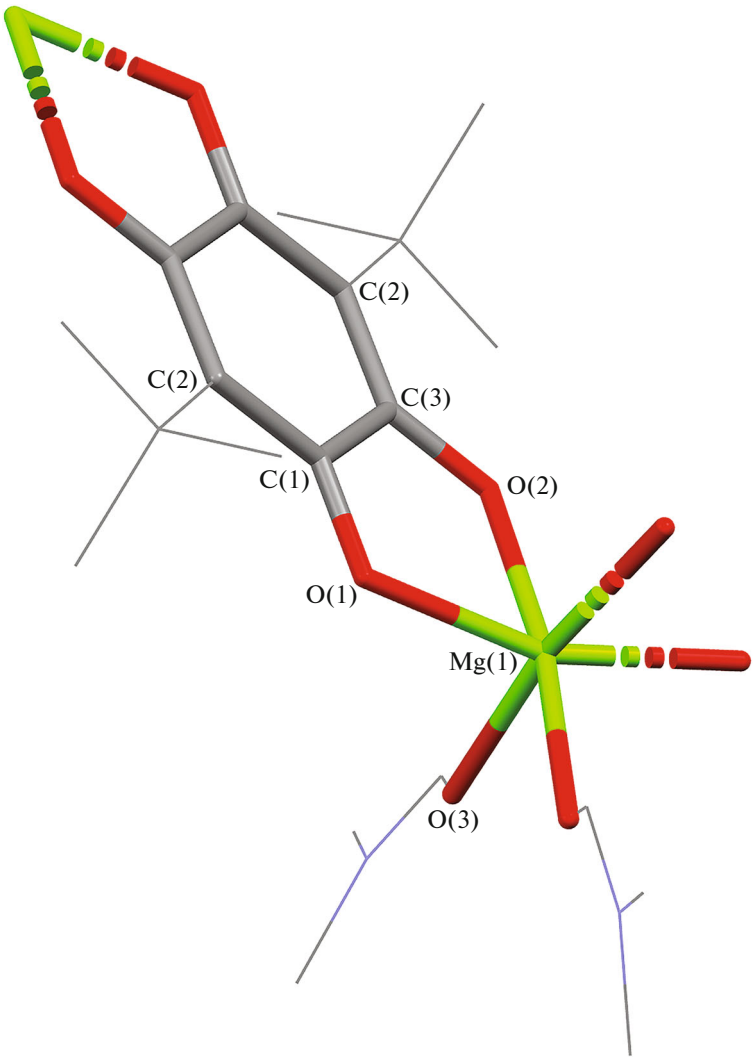

Fig. 2. Structure of the repeated unit of MOF **I**.

The Mg–O bonds with the anilate ligands are nearly equalized ranging from 2.04 to 2.07 Å, which does not exceed the sum of covalent radii of the corresponding elements (2.24 Å) [33]. It is typical that the coordination of the neutral donor ligands (DMF in **I** and NMP in **III**) is characterized by the magnesium–oxygen bond lengths comparable with Mg–O(pQ). This indicates the formation of strong coordination bonds, which, as shown by the TG analysis, decompose at fairly high temperatures.

The thermal stability of MOF **I**–**III** was evaluated by the TG and DSC methods (Fig. 4). According to the data of these methods for MOF **I**, 1.5 DMF molecules decoordinate from the metal atom in a temperature range of 120–220°C with a mass loss of 26%. The further heating to 330°C results in the elimination of the remained DMF (0.5 molecule) and transformation of the pQ^{2-} ligand with the detachment of two isobutylene molecules due to the destruction of the *tert*-butyl substituents with the total mass loss equal to 34%. The final decomposition of the polymer occurs further. A similar behavior is observed on heating for MOF **II**, and the distinction is that the decoordination of only one DMAA molecule occurs in a temperature range of 120–190°C with a mass loss of 20%. Heating to 350°C results in the elimination of one more DMAA molecule from the magnesium atom and in the destruction of the organic ligand similarly to compound **I**. The mass loss in the second step of the TG curve for compound **II** is 44%. According to the TG data, MOF **III** contains the occluded solvent, which is removed from the sample in the temperature range from 50 to 100°C (10% mass loss corresponds to 0.5 NMP molecule). The second step in the TG curve (120–200°C, mass loss 19%) corresponds to the removal of one coordinated NMP molecule and destruction of the organic ligands similarly to compounds **I** and **II**. The mass loss in the third step of the TG curve is 38%.

Table 1. Crystallographic data and experimental and structure refinement parameters for complexes **I** and **III**

Parameter	Value	
	I	**III**
T, K	100 K	
Crystal system	Monoclinic	
Space group	$C2/c$	$P2_1/c$
a, Å	10.616(2)	12.8342(13)
b, Å	16.897(3)	17.4410(10)
c, Å	12.483(3)	12.4170(18)
β, deg	90.858(16)	114.699(10)
V, Å^3	2238.9(8)	2525.2(5)
Z	4	
ρ_{calc}, g/cm^3	1.248	1.244
μ, mm^{-1}	0.153	0.145
θ_{min}–θ_{max}, deg	2.690–30.720	1.949–30.962
Number of observed reflections	12290	38665
Number of independent reflections	2482	5748
R_{int}	0.0310	0.0778
$S(F^2)$	1.085	1.045
R_1/wR_2 ($I > 2\sigma(I)$)	0.0440/0.1183	0.0533/0.1399
R_1/wR_2 (for all parameters)	0.0539/0.1271	0.0802/0.1569
Absorption coefficient	0.022(3)	0.0077(14)
$\Delta\rho_{max}/\Delta\rho_{min}$, e Å^{-3}	0.255/–0.478	0.393/–0.304

Coordination polymers **I**–**III** are insoluble in water and organic solvents. Therefore, the EAS in the UV-visible range of the studied magnesium MOF were detected for suspensions in mineral oil and are presented in Fig. 5. The spectra of all compounds exhibit intense bands at 310–320 and 335–345 nm and broad absorption bands in a longer-wavelength spectral range at λ ≈ 500 nm (515 (**I**), 510 (**II**), and 490 nm (**III**)). This character of the EAS was observed earlier for the lanthanide 2D MOF based on this anilate ligand [23].

The obtained spectral characteristics are in good agreement with the quantum-chemical calculation results performed at the B3LYP/6-311+(d,p) level. The monomeric unit of compound **I** was chosen for the calculations, representing in the experimental geometry the doubly charged cation $[(H_2O)_2L_2(Mg\text{-}pQ)MgL_2(H_2O)_2]^{2+}$ in which water molecules occupy the positions of the oxygen atoms of the bridging anilate ligands. The frontier molecular orbitals in the model dication (Fig. 6) are localized on the redox-active ligand. The intraligand electron transfer highest occupied molecular orbital (HOMO)–lowest unoccupied molecular orbital (LUMO) determines the long-wavelength absorption band (λ = 515 nm) in the EAS of compound **I**, and the difference in energies of the frontier orbitals (2.9 eV) is well consistent with the position of this broad absorption band observed in the

Table 2. Selected bond lengths (Å) in complexes **I** and **III**

Bond (*d*, Å)	**I**	**III**
Mg(1)–O(1)	2.0426(11)	2.0514(14)
Mg(1)–O(2)	2.0646(12)	2.0694(15)
Mg(1)–O(3)	2.0578(12)	2.058(5)
Mg(1)–O(4)		2.072(3)
Mg(1)–O(5)		2.0458(14)
Mg(1)–O(6)		2.0749(15)
O(1)–C(1)	1.2662(18)	1.270(2)
O(2)–C(3)	1.2635(18)	1.256(2)
O(5)–C(8)		1.267(2)
O(6)–C(10)		1.261(2)
C(1)–C(2)	1.409(2)	1.392(3)
C(1)–C(3)	1.553(2)	1.555(2)
C(2)–C(3)	1.405(2)	1.411(2)
C(8)–C(9)		1.399(3)
C(8)–C(10)		1.552(2)
C(9)–C(10)		1.412(3)

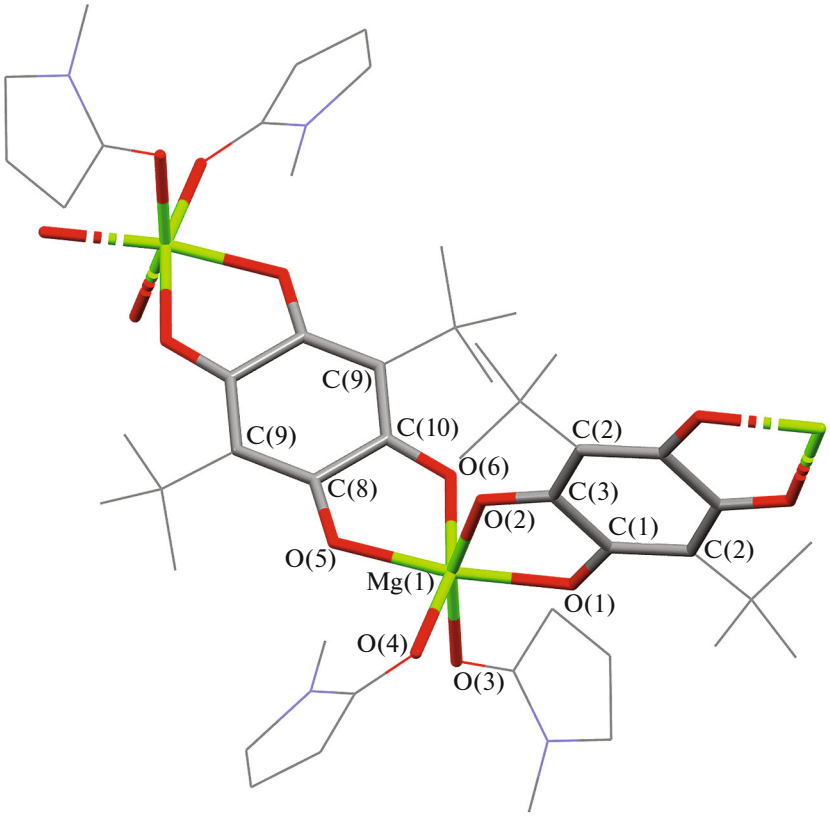

Fig. 3. Structure of the repeated unit of MOF **III**.

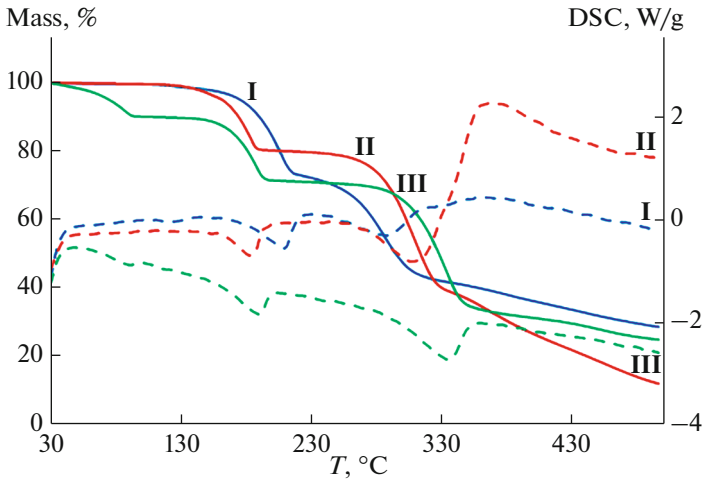

Fig. 4. TG (solid lines) and DSC (dashed lines) curves for complexes **I**–**III**.

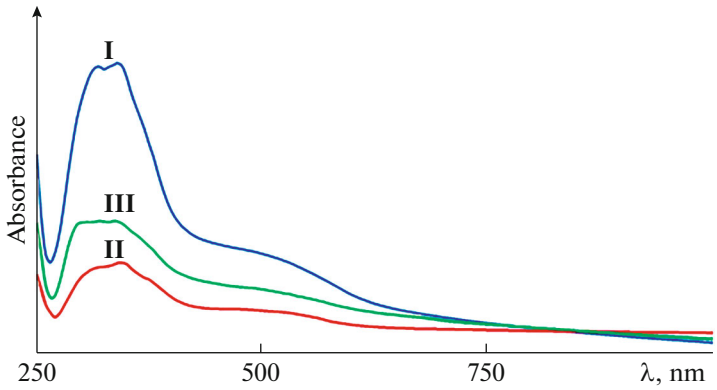

Fig. 5. Electronic absorption spectra of complexes **I**–**III**.

experimental spectrum. It should be mentioned that the bridging mode of pQ^{2-} anilate ligand binding to the magnesium ions in compounds **I**–**III** is accompanied by the approaching of the frontier orbitals by ~0.35 eV compared to the antimony(V) complex in which this redox-active ligand exists in the *o*-quinoid form. Taking into account that the frontier orbitals do not involve the solvent molecules coordinated to magnesium, we can assert that the conclusions made for complex **I** would be valid for compounds **II** and **III**.

Thus, one-dimensional magnesium MOF based on the redox-active anilate ligand (2,5-dihydroxy-3,6-di-*tert*-butyl-*para*-benzoquinone) were first synthesized in this work. According to the TG data, the synthesized compounds are characterized by high thermal stability. The results of the spectral study and quantum-chemical calculations indicate that the intense color of the synthesized compounds is due to the intraligand charge transfer.

ACKNOWLEDGMENTS

The studies were carried out using the equipment of the Analytical Center of the Razuvaev Institute of Organometallic Chemistry (Russian Academy of Sciences). Electronic absorption spectra recording was supported by the Ministry of Science and Higher Education of the Russian Federation using the scientific equipment of the Scientific Technical Center for Raman Spectroscopy of the Nesmeyanov Institute of Organoelement Compounds (Russian Academy of Sciences). The X-ray diffraction data were obtained on the Belok beamline at the Kurchatov specialized source of synchrotron radiation of the Kurchatov Institute Russian Research Center.

FUNDING

This work was supported by the Russian Foundation for Basic Research, project no. 18-29-04041-mk.

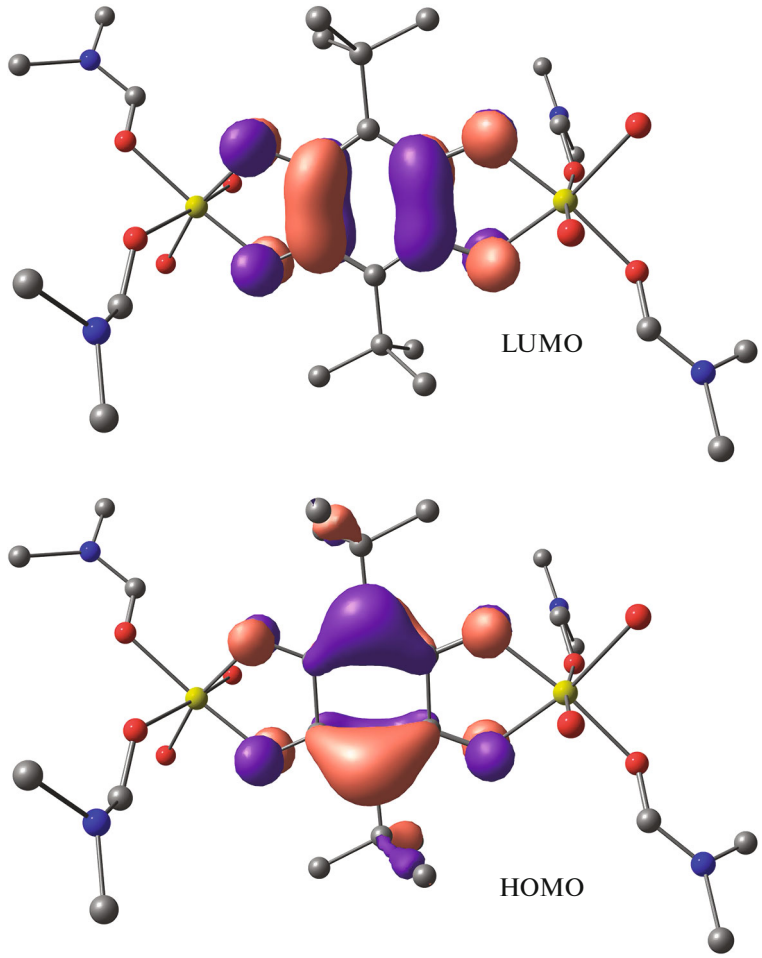

Fig. 6. Frontier orbitals for the model $(H_2O)_2L_2(MgpQ)MgL_2(H_2O)_2]^{2+}$ dication.

CONFLICT OF INTEREST

The authors declare that they have no conflicts of interest.

REFERENCES

1. Kingsbury, C.J., Abrahams, B.F., Auckett, J.E., et al., *Chem.-Eur. J.*, 2019, vol. 25, p. 5222.
2. Abrahams, B.F., Dharma, A.D., Dyett, B., et al., *Dalton Trans.*, 2016, vol. 45, p. 1339.
3. Sahadevan, S.A., Monni, N., Oggianu, M., et al., *ACS Appl. Nano Mater.*, 2020, vol. 3, p. 94.
4. Artizzu, F., Atzori, M., Liu, J., et al., *J. Mater. Chem.*, 2019, vol. 7, p. 11207.
5. Wang, Y., Liu, X., Li, X., et al., *J. Am. Chem. Soc.*, 2019, vol. 141, p. 8030.
6. Chang, C.-H., Li, A.-C., Popovs, I., et al., *J. Mater. Chem. A*, 2019, vol. 7, p. 23770.
7. Bondaruk, K. and Hua, C., *Cryst. Growth Des.*, 2019, vol. 19, p. 3338.
8. Calbo, J., Golomb, M.J., and Walsh, A., *J. Mater. Chem. A*, 2019, vol. 7, p. 16571.
9. Wang, M., Dong, R., and Feng, X., *Chem. Soc. Rev.*, 2021, vol. 50, p. 2764. https://doi.org/10.1039/d0cs01160f
10. Martínez-Hernández, C., Gómez-Claramunt, P., Benmansour, S., et al., *Dalton Trans.*, 2019, vol. 48, p. 13212.
11. Liu, L., DeGayner, J.A., Sun, L., et al., *Chem. Sci.*, 2019, vol. 10, p. 4652.
12. Chen, J., Sekine, Y., Komatsumaru, Y.S., et al., *Angew. Chem., Int. Ed. Engl.*, 2018, vol. 57, p. 12043.
13. Mercuri, M.L., Congiu, F., Concas, G., et al., *Magnetochemistry*, 2017, vol. 3, p. 1.
14. Benmansour, S. and Gómez-García, C.J., *Polymers*, 2016, vol. 8, p. 89.
15. Huang, Z., Yu, H., Wang, L., et al., *Coord. Chem. Rev.*, 2021, vol. 430, p. 213737.
16. Kitagawa, S. and Kawata, S., *Coord. Chem. Rev.*, 2002, vol. 224, p. 11.
17. D'Alessandro, D.M., *Chem. Commun.*, 2016, vol. 52, p. 8957.
18. Benmansour, S. and Gómez-García, C.J., *Magnetochemistry*, 2020, vol. 6, p. 71.

19. Khamaletdinova, N.M., Meshcheryakova, I.N., Piskunov, A.V., et al., *J. Struct. Chem.*, 2015, vol. 56, p. 233.
20. Okhlopkova, L.S., Poddel'sky, A.I., Smolyaninov, I.V., Fukin, G.K., *Russ. J. Coord. Chem.*, 2020, vol. 46, no. 6, p. 386. https://doi.org/10.1134/S107032842005005X
21. Min, K.S., DiPasquale, A.G., Rheingold, A.L., et al., *J. Am. Chem. Soc.*, 2009, vol. 131, p. 6229.
22. Min, K.S., DiPasquale, A., Rheingold, A.L., et al., *Inorg. Chem. Commun.*, 2007, vol. 46, p. 1048.
23. Kharitonov, A.D., Trofimova, O.Y., Meshcheryakova, I.N., et al., *CrystEngComm*, 2020, vol. 22, p. 4675.
24. Frisch, M.J., Trucks, G.W., Schlegel, H.B., et al., Wallingford: Gaussian, Inc., 2013.
25. Becke, A.D., *J. Chern. Phys.*, 1993, vol. 93, p. 1372.
26. Svetogorov, R.D., Dorovatovskii, P.V., and Lazarenko, V.A., *Cryst. Res. Technol.*, 2020, vol. 55, p. 1900184.
27. Kabsch, W., *Acta Crystallogr., Sect. D: Biol. Crystallogr.*, 2010, vol. 66, p. 125.
28. Sheldrick, G.M., *Acta Crystallogr., Sect. C: Struct. Chem.*, 2015, vol. 71, p. 3.
29. Dolomanov, O.V., Bourhis, L.J., Gildea, R.J., et al., *J. A`pl. Crystallogr.*, 2009, vol. 42, p. 339.
30. Turner, M.J., McKinnon, J.J., Wolff, S.K., et al., *CrystalExplorer17*, University of Western Australia, 2017.
31. Piskunov, A.V., Maleeva, A.V., Bogomyakov, A.S., et al., *Russ. Chem. Bull.*, 2017, vol. 66, p. 1618.
32. Piskunov, A.V., Lado, A.V., Abakumov, G.A., et al., *Russ. Chem. Bull.*, 2007, vol. 56, no. 1, p. 97.
33. Batsanov, S.S., *Russ. J. Inorg. Chem.*, 1991, vol. 36, p. 1694.

Translated by E. Yablonskaya